Available online at www.sciencedirect.com
SCIENCE DIRECT®
Cryogenics 45 (2005) 163–172
Cryogenics
www.elsevier.com/locate/cryogenics

Numerical calculation of the temperature difference between the extremities of a thermoacoustic stack plate

D. Marx *, Ph. Blanc-Benon

Centre acoustique, LMFA & UMR CNRS 5509, Ecole Centrale de Lyon, 36 avenue Guy de Collongue, 69134 Ecully Cedex, France

Received 20 October 2003; received in revised form 27 October 2003; accepted 6 August 2004

Abstract

When a plate is placed in a thermoacoustic resonator, one extremity of the plate heats up while the other cools down due to the thermoacoustic effect. In the present work the temperature difference between the extremities of the plate is calculated numerically. The computed temperature difference is compared to the one predicted by the linear theory. Some discrepancies are found even at low acoustic Mach numbers. These discrepancies can not be attributed to non-linear effects, rather they exist because of thermal effects. In particular the mean temperature in the fluid and in the plate are not equal. The discrepancies can be eliminated using corrective coefficients. Some deviations between the linear theory predictions and numerical results also occur at higher Mach numbers and are due to non-linearities, and especially temperature non-linearities that are generated in the vicinity of the plate.

PACS: 43.35.Ud
Keywords: Thermoacoustics; Thermoacoustic refrigerator; Numerical simulation

1. Introduction

Thermoacoustic engines and refrigerators physics has been reviewed by Swift [1]. Both kinds of devices may be used in cryogenic technology. A design methodology for loudspeaker-driven thermoacoustic refrigerators has been provided by Tijani et al. [2] in the view of cryogenic applications. The targeted temperature of their refrigerator is −65 °C, and can be achieved at a modest drive ratio $D_r = 3\%$. The drive ratio is an important parameter in thermoacoustics and is defined as the ratio of the pressure maximum amplitude in the resonator, divided by the mean pressure. A thermo-driven refrigerator was built by Tu et al. [3]. In their device, a thermoacoustic refrigerator part was driven by the acoustic wave created in a thermoacoustic engine part. The measured temperature difference was about 10 °C, a low value obtained at $D_r = 1.5\%$. The value for the temperature difference could be increased by increasing the drive ratio. Jin et al. [4] built a cooler in which a pulse tube is driven by a thermoacoustic engine. This device could reach low temperatures, about 120 K.

When a thermoacoustic device has to be designed, the major theory to rely upon is the linear theory [1]. This theory is the basis for the design methodology of Tijani et al. [2], as well as that for the analytical predictions of Tu et al. [3]. Yet, the limits of this theory are not firmly established, especially as the drive ratio is increased in order to increase acoustic power and decrease the minimum achievable temperature. The present work is a contribution to the study of the limitations of the linear theory. These limits are investigated in the simple case of a plate placed in a stationary acoustic wave. As the objective is above all to improve the understanding of

* Corresponding author. Tel.: +33 4 72 18 60 18; fax: +33 4 72 18 91 43.
E-mail address: david.marx@ec-lyon.fr (D. Marx).

0011-2275/$ - see front matter © 2004 Elsevier Ltd. All rights reserved.
doi:10.1016/j.cryogenics.2004.08.007

the physics underlying the thermoacoustic effect, no cryogenic temperature is targeted in this work.

When a plate is placed in a stationary acoustic wave, one extremity of the plate heats up while the other cools down due to the thermoacoustic effect [1]. Once a stationary state is reached, the temperature difference ΔT between the plate extremities may be calculated using the linear theory, assuming that the thermoacoustic heat flux carried along the plate is balanced by conductive return heat fluxes in the plate and in the fluid [5]. Several authors made a study of this temperature difference either experimentally or numerically and have made comparisons with the linear theory predictions, but all studies do not reach the same conclusions. In the studies of Atchley et al. [6] and Worlikar et al. [7] agreement were found with the linear theory at low Mach numbers, while a disagreement appeared at higher Mach numbers due to non-linear effects. The acoustic Mach number $Ma = u_A/c$ is defined as the ratio of maximum velocity amplitude u_A in the resonator divided by the speed of sound c. It is related to the drive ratio D_r by $Ma = D_r/\gamma$, where γ is the ratio of specific heats. Atchley et al. and Worlikar et al. found that the disagreement between their results and the linear theory occurs when the Mach number exceeds 1%. One interesting remark is that the simulation of Worlikar is performed in the vicinity of the plate, hence non-linear effects responsible for the observed disagreement are unlikely to be due to non-linear wave propagation in the resonator. Another interesting feature is that the agreement between experiments and theory is better near velocity node than near velocity antinode at high Mach numbers [6]. Some other experiments performed by Kim et al. [8], Duffourd [9], and Piccolo et al. [10] could not match the linear theory predictions even at low Mach numbers, and discrepancies up to 300% were reported. Although temperature differences measured in steady states by Piccolo et al. do not match the linear theory predictions, measurements made in the transient regime indicated that the thermoacoustic heat flux carried by the plate is well predicted. This result shows that the disagreement concerning the temperature difference in the stationary state is not necessarily due to non-linear effects, but rather to other thermal effects. In the present work, a numerical simulation is performed, and the temperature difference between the extremities of the plate is compared to the linear theory prediction. In the configuration that is studied, a slight disagreement is found at low Mach numbers, which can be attributed to thermal effects. At higher Mach numbers a bigger disagreement is found which is due to non-linear effects and in particular to temperature non-linearities.

In the following some details are first provided about the numerical simulation. Then formulas giving the temperature difference predicted by the linear theory are recalled. Some results on non-linear effects useful for discussion are then given. Finally results on temperature difference obtained with the simulation are compared to the linear theory predictions and conclusions are drawn.

2. Numerical modelling

The thermoacoustic refrigerator considered here is shown in Fig. 1. The resonator length is half the wavelength λ. The computational domain is referred to as CD and is shown in Fig. 2. It is located between $x = x_{inout}$ *and the resonator end at* $x = l_{res} = \lambda/2$. We take advantage of the stack periodicity in the y direction so that we include only one 1D stack plate in the domain. We also enforce symmetry conditions on the lateral boundaries. The height of the domain y_0 is half the plate spacing in the stack. C is the cold side of the plate, H is its hot side, and S is the stack plate center. L is the length of the plate. An incident travelling wave is injected into the domain through the section S_{inout} located at $x = x_{inout}$ using characteristics method [11]. The wave travels through the domain and is reflected at the resonator end. The reflected wave travels in the direction of the source and leaves the domain through S_{inout}. The superimposition of the incident and reflected waves results in the standing wave phasing that is required in a thermoacoustic refrigerator. The total distance the wave travels in the domain being less than a wavelength, there is no time for non-linear distorsion. Hence the standing wave is nearly harmonic, even at high Mach numbers.

The following equations are solved for the flow:

$$p = \rho r T \tag{1}$$

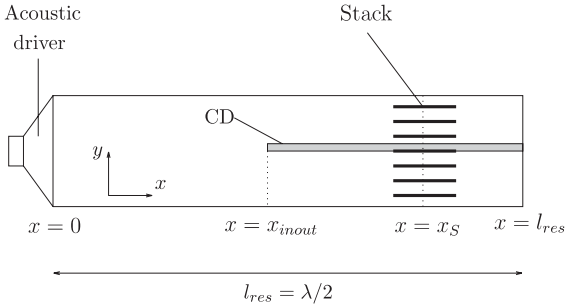

Fig. 1. Sketch of the thermoacoustic refrigerator. CD is the computational domain.

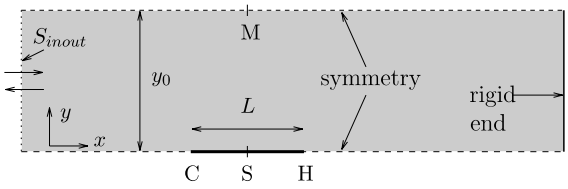

Fig. 2. Computational domain CD. C is the cold side of the plate, and H is its hot side.

$$\frac{\partial \rho}{\partial t} + \nabla \cdot (\rho \mathbf{u}) = 0 \tag{2}$$

$$\frac{\partial (\rho \mathbf{u})}{\partial t} + \nabla \cdot (\rho \mathbf{u}\mathbf{u}) + \nabla p = \nabla \cdot \boldsymbol{\tau} \tag{3}$$

$$\frac{\partial T}{\partial t} + \mathbf{u} \cdot \nabla T + (\gamma - 1) T \nabla \cdot \mathbf{u} = \frac{(\gamma - 1)}{\rho r} (\Phi + \nabla \cdot (K \nabla T)) \tag{4}$$

T, ρ, and p are respectively the temperature, the density, and the pressure of the fluid. $\mathbf{u}$ is the velocity vector, $\boldsymbol{\tau}$ is the stress tensor, and Φ is the viscous dissipation. We note K the thermal conductivity of the fluid, $r = 287\,\mathrm{J\,K^{-1}\,kg^{-1}}$ the gas constant, and we take $\gamma = 1.4$. The 1D equation for the plate temperature T_s is

$$\rho_s c_s \frac{\partial T_s}{\partial t} = \nabla \cdot (K_s \nabla T_s) + \frac{K}{l} \left(\frac{\partial T}{\partial y} \right)_{\text{plate}} \tag{5}$$

ρ_s, c_s and K_s are respectively the density, the specific heat and the thermal conductivity of the plate. l is half the thickness that an equivalent 2D plate would have. The second term on the right hand side of Eq. (5) represents the coupling with the flow. In deriving this term use has been made of the continuity of temperature and heat flux at the plate surface. On the plate surface, the boundary condition $T = T_s$ is enforced.

Eqs. (1)–(4) for the fluid together with Eq. (5) for the plate are solved using a fourth order Runge–Kutta time integration. Spatial derivatives are calculated using fourth order finite differences. These schemes are high order schemes and are not very dissipative. Hence some grid to grid oscillations are likely to appear, there are suppressed with a selective filtering. Those methods are classical methods which are usually used for aeroacoustic computations [12]. More details about the numerical methods used in the present simulation have been given elsewhere [11,13].

The computational cost of the numerical simulation of a thermoacoustic refrigerator is high due to length scale disparity ($l_{\text{res}} \gg L \gg y_0$) [11]. Fortunately it has been shown [11] that the computational cost is inversely proportional to the operating frequency f of the refrigerator. In the following we use $f = 20\,\mathrm{kHz}$, which corresponds to a wavelength $\lambda = 17\,\mathrm{mm}$. Choosing such a high frequency does not affect the physics of the problem [14].

3. Background of linear theory

The temperature difference $\Delta T = T_s(H) - T_s(C)$ between the extremities of the plate is obtained assuming a zero mean total energy flux along the plate. In stationary state it is possible to write [1,5]:

$$\dot{E}_m = \dot{Q}_{\text{thermoac,m}} + \dot{W}_m + \dot{Q}_{\text{cond,m}} = 0, \tag{6}$$

where $\dot{E}_m$ is the mean energy flux. Subscript m indicates mean (time-averaged) quantities. Eq. (6) indicates that the thermoacoustic heat flux $\dot{Q}_{\text{thermoac,m}}$ and the work flux $\dot{W}_m$ are balanced by the conductive return heat flux $\dot{Q}_{\text{cond,m}}$. The conductive heat flux can be written in the form:

$$\dot{Q}_{\text{cond,m}} = -K y_0 \frac{\mathrm{d}T_m}{\mathrm{d}x} - K_s l \frac{\mathrm{d}T_m}{\mathrm{d}x}. \tag{7}$$

$\dot{W}_m$ is not taken into account by Wheatley et al. [5], which introduces few differences with the present formulation, $\dot{W}_m$ being small. Starting from Eq. (6) and using Eq. (55) of Swift [1] for $\dot{E}_m$, the following formula for the temperature difference $\Delta T = L \mathrm{d}T_m/\mathrm{d}x$ is obtained:

$$\Delta T = \frac{-L y_0}{4 \rho_m c} P_A^2 \sin(2 k x_S) A_1 \times \left[y_0 K + l K_s - \frac{y_0 c_p}{4 \omega \rho_m c^2 (1 - Pr)} P_A^2 (1 - \cos(2 k x_S)) A_2 \right]^{-1}, \tag{8}$$

where A_1 et A_2 are given by

$$A_1 = \mathrm{Im}\left[\left(1 - f_v^* - \frac{f_\kappa - f_v^*}{(1 + \epsilon_s)(1 + Pr)} \right) \frac{1}{1 - f_v^*} \right], \tag{9}$$

$$A_2 = \mathrm{Im}\left[\left(f_v^* + \frac{(f_\kappa - f_v^*)(1 + \epsilon_s f_v / f_\kappa)}{(1 + \epsilon_s)(1 + Pr)} \right) \frac{1}{(1 - f_v)(1 - f_v^*)} \right]. \tag{10}$$

We note $k = 2\pi/\lambda$ the wave number, $\omega = 2\pi f$ the angular frequency, Pr the Prandtl number, c_p the isobaric specific heat. x_S is the plate center position in the resonator (see Fig. 1). $P_A = \rho_m c u_A$ is the maximal amplitude of the pressure oscillation in the resonator. The quantities f_v, f_κ, and ϵ_s depend on fluid and solid properties and on geometry, they are given by Swift [1]:

$$f_v = \frac{\tanh[(1 + \mathrm{i}) y_0 / \delta_v]}{(1 + \mathrm{i}) y_0 / \delta_v}, \tag{11}$$

$$f_\kappa = \frac{\tanh[(1 + \mathrm{i}) y_0 / \delta_\kappa]}{(1 + \mathrm{i}) y_0 / \delta_\kappa}, \tag{12}$$

$$\epsilon_s = \epsilon_0 \frac{\tanh[(1 + \mathrm{i}) y_0 / \delta_\kappa]}{\tanh[(1 + \mathrm{i}) l / \delta_{\kappa,s}]}, \tag{13}$$

where

$$\epsilon_0 = \frac{\rho_m c_p \delta_\kappa}{\rho_s c_s \delta_{\kappa,s}}. \tag{14}$$

In these equations the viscous penetration depth δ_v in the fluid, the thermal penetration depth δ_κ in the fluid, and the thermal penetration depth $\delta_{\kappa,s}$ in the solid plate are given by

$$\delta_\nu = \sqrt{\frac{2\nu}{\omega}}, \quad \delta_\kappa = \sqrt{\frac{2\kappa}{\omega}}, \quad \delta_{\kappa,\mathrm{s}} = \sqrt{\frac{2\kappa_\mathrm{s}}{\omega}}, \tag{15}$$

where ν is the fluid kinetic viscosity, $\kappa = K/\rho c_p$ is the fluid thermal diffusivity, and $\kappa_\mathrm{s} = K_\mathrm{s}/\rho_\mathrm{s} c_\mathrm{s}$ is the solid thermal diffusivity. The symbol $*$ denotes the complex conjugate. For Eq. (8) to be valid, the length L of the plate must be small in comparison with the wave length λ (short stack approximation). Usual assumptions of the linear theory are also made [1]. In particular, it is assumed that the mean temperature gradient $\mathrm{d}T_\mathrm{m}/\mathrm{d}x = \Delta T/L$ is the same in the plate and in the fluid. Relation (8) also assumes that this gradient is constant along the plate. Note that the "boundary layer" approximation ($y_0/\delta_\nu \gg 1$) has not been used. In that approximation the coefficients A_1 and A_2 should be replaced respectively by $A_{1,\mathrm{bla}}$ and $A_{2,\mathrm{bla}}$ given by the following analytical relations:

$$A_{1,\mathrm{bla}} = \frac{\delta_\kappa}{2y_0} \frac{1 - \frac{\delta_\nu}{y_0} + \sqrt{Pr}}{(1+\epsilon_0)(1+Pr)\left(1 - \frac{\delta_\nu}{y_0} + \frac{1}{2}\left(\frac{\delta_\nu}{y_0}\right)^2\right)}, \tag{16}$$

$$A_{2,\mathrm{bla}} = -\frac{\delta_\kappa}{2y_0} \times \frac{(1-Pr)(1+\sqrt{Pr}+Pr+Pr\epsilon_0)}{(1+\sqrt{Pr})(1+\epsilon_0)(1+Pr)\left(1 - \frac{\delta_\nu}{y_0} + \frac{1}{2}\left(\frac{\delta_\nu}{y_0}\right)^2\right)}. \tag{17}$$

Relations (16) and (17) are very good approximations to relations (9) and (10) as soon as $y_0/\delta_\nu > 2$. In what follows, results of the simulation are compared to predictions of Eqs. (8)–(10).

4. Non-linear effects

We previously insisted on the fact that the method used in our simulations to sustain an acoustic wave in the domain allows to get a high level stationary acoustic wave, yet nearly harmonic. This is now illustrated. The incident wave entered into the domain through the section S_inout with the characteristics method corresponds to the following expression for the acoustic pressure variation:

$$p'(x,t) = \gamma Map_0 \sin\left(k(x - x_\mathrm{inout}) - \omega t\right) \tag{18}$$

Here and in the following the prime indicates the perturbation of a quantity while the subscript 0 represents its value at rest. Hence any quantity ψ is written in the form:

$$\psi = \psi_0 + \psi' \tag{19}$$

In the linear approximation, the stationary wave resulting from the superposition of this wave and the reflected wave on the rigid end of the domain at $x = l_\mathrm{res}$ can be predicted analytically, and corresponds to the following expression for the pressure:

$$p'(x,t) = \gamma Map_0 \cos\left(k(x - l_\mathrm{res})\right) \sin\left(k(l_\mathrm{res} - x_\mathrm{inout}) - \omega t\right) \tag{20}$$

Some numerical simulations are made without including the stack plate in the domain. Two Mach numbers are used and the acoustic pressure obtained in the domain is compared to Eq. (20) for eight instants within one period τ. Fig. 3 presents the results for a low Mach number value $Ma = 0.5\%$, and Fig. 4 presents the results for a high Mach number value $Ma = 8\%$. For $Ma = 0.5\%$ (Fig. 3), the calculated pressure and the one given by Eq. (20) agree perfectly. This agreement is expected because non-linear effects are negligible at low Mach numbers. This also partially validates the numerical methods used here. For $Ma = 8\%$ (Fig. 4), some deviations are observed. They are due to non-linear propagation of the high pressure wave in the domain. Nevertheless the deviation is small given the high value of the Mach number. The time variation of the pressure at the end of the resonator for $Ma = 8\%$ is given in Fig. 5. We observe little deviations from a perfect harmonic variation. For this value of the Mach number, the time variation of pressure for an acoustic wave that would be sustained by a piston at $x = 0$ would present shocks. Hence the method allows us to use very high Mach numbers without creating a lot of harmonics. This is accomplished in a very simple way, and in a constant cross-section computational domain. Note that if a piston were used at $x = 0$, such a result could be obtained only with an anharmonic tube, for example a tube of non-constant cross-section [15].

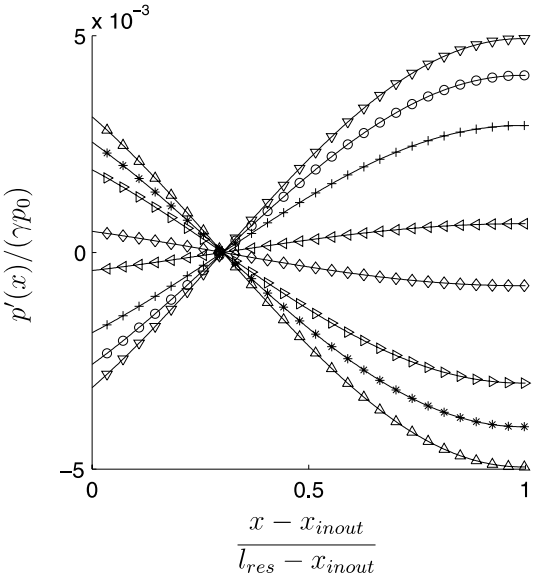

Fig. 3. Acoustic pressure along the computational domain for several instants within one period τ: (○) $t = 0$, (▽) $t = \tau/8$, (+) $t = 2\tau/8$, (◇) $t = 3\tau/8$, (*) $t = 4\tau/8$, (△) $t = 5\tau/8$, (▷) $t = 6\tau/8$, (◁) $t = 7\tau/8$, (—) theoretical expression (Eq. (20)). $Ma = 0.5\%$.

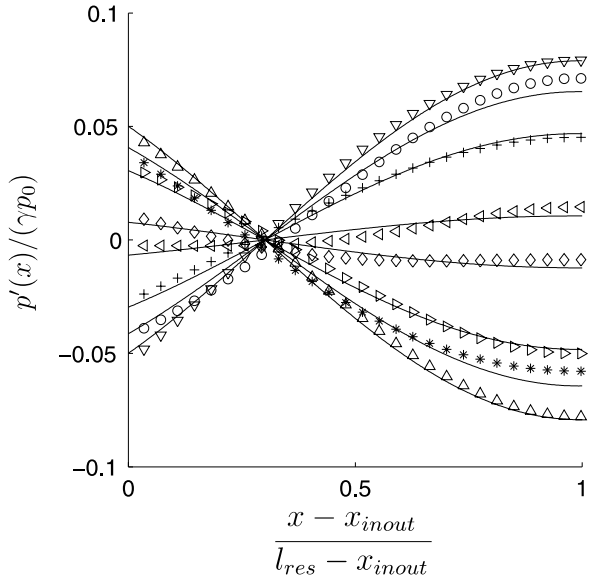

Fig. 4. Acoustic pressure along the computational domain for several instants within one period τ: (○) $t = 0$, (▽) $t = \tau/8$, (+) $t = 2\tau/8$, (◇) $t = 3\tau/8$, (∗) $t = 4\tau/8$, (△) $t = 5\tau/8$, (▷) $t = 6\tau/8$, (◁) $t = 7\tau/8$, (—) theoretical expression (Eq. (20)). $Ma = 8\%$.

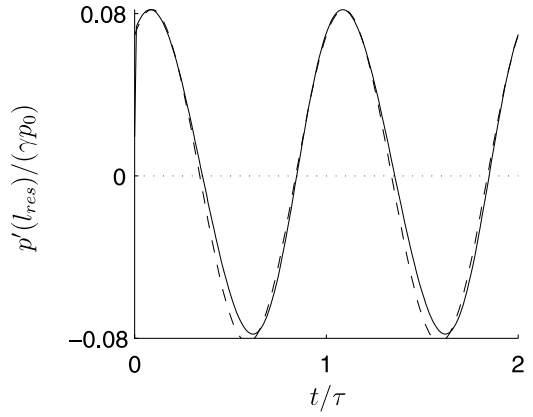

Fig. 5. Time variation of the acoustic pressure (—) at the rigid end of the domain ($x = l_{res}$). Two periods τ are shown. $Ma = 8\%$. The dashed line (– –) is a perfect harmonic curve.

In a previous study some non-linearities were found at high Mach numbers [11]. These non-linearities do not arise due to non-linear propagation given the method used to sustain the wave and the results presented just above. Hence the kind of non-linearities that are observed are different from the one reported by Atchley et al. [16], which are due to non-linear propagation in the resonator. In the present case non-linearities are due to the presence of the stack plate. They are observed above the stack, but not in the other parts of the resonator. In particular it was shown that at high Mach numbers, the temperature oscillation is non-linear above the plate, whereas the velocity oscillation remains nearly harmonic. This behaviour is in agreement with analytical prediction made by Gusev et al. [17]. These authors show that the temperature oscillation in the stack region can be highly non-linear due to the transition from an adiabatic behaviour just outside the plate to an isothermal behaviour above the plate. Furthermore the non-linear behaviour was found to be stronger near velocity antinodes and for short plates, thus showing that velocity and particle displacement are involved in the process [11]. As an example, the velocity and temperature time variations at point M of the computational domain (see Fig. 2) are given at a high Mach number, $Ma = 8\%$, for three different positions of the plate, which is taken to be isothermal. The plate position is indicated by the dimensionless number kx_S. Results for a plate located at $kx_S = 2.13$ (near the velocity antinode) are

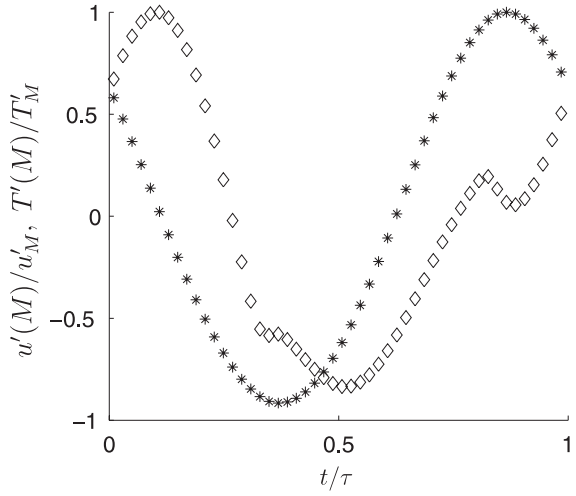

Fig. 6. Time variation of the temperature T'(M) and the velocity u'(M) at point M of the computational domain: (∗) velocity, (◇) temperature. Curves are normalized using maximal velocity u'_M and temperature T'_M at point M. $Ma = 8\%$, $L = \lambda/40$, $y_0/\delta_\kappa = 2.45$, and $kx_S = 2.13$.

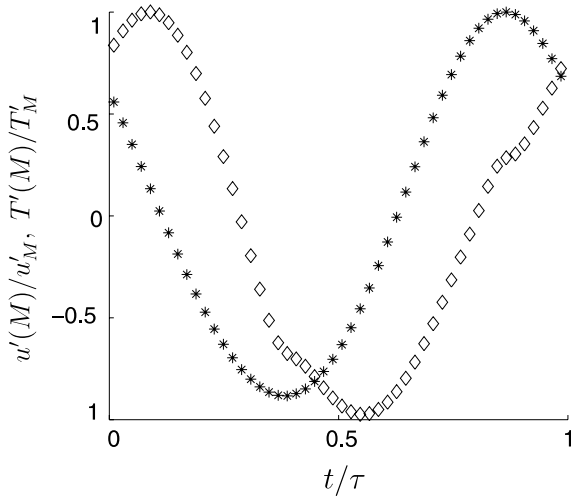

Fig. 7. Time variation of the temperature T'(M) and the velocity u'(M) at point M of the computational domain: (∗) velocity, (◇) temperature. Curves are normalized using maximal velocity u'_M and temperature T'_M at point M. $Ma = 8\%$, $L = \lambda/40$, $y_0/\delta_\kappa = 2.45$, and $kx_S = 2.35$.

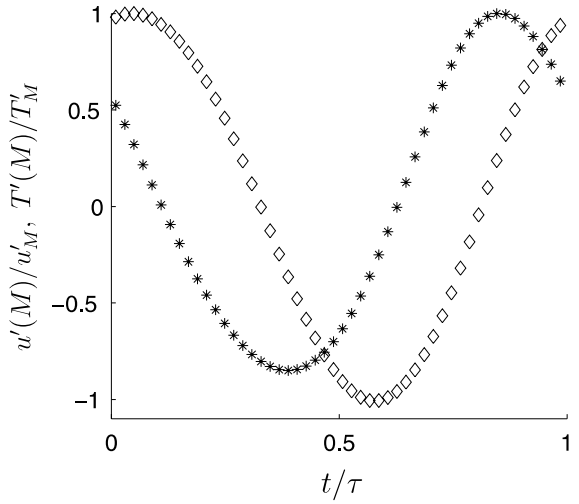

Fig. 8. Time variation of the temperature T'(M) and the velocity u'(M) at point M of the computational domain: (∗) velocity, (◇) temperature. Curves are normalized using maximal velocity u'_{M} and temperature T'_{M} at point M. $Ma = 8\%$, $L = \lambda/40$, $y_0/\delta_\kappa = 2.45$, and $kx_{\mathrm{S}} = 2.81$.

given in Fig. 6. Those for a plate located at $kx_{\mathrm{S}} = 2.35$ (middle position between the velocity antinode and the pressure antinode) are given in Fig. 7. Finally those for a plate located at $kx_{\mathrm{S}} = 2.81$ (near the pressure antinode) are given in Fig. 8. As was indicated above, we observe that the temperature time variation is strongly non-harmonic for a plate located near the velocity antinode, while the velocity time variation remains nearly harmonic (Fig. 6). The non-harmonic behaviour of the temperature decreases when the plate is pushed toward the velocity node, that is toward $kx_{\mathrm{S}} = 3.14$ (Figs. 7 and 8). In Section 5, this behaviour is related to the one observed for the temperature difference.

5. Temperature difference between the plate extremities

In this section simulations are performed and the temperature difference between the plate extremities is compared to the linear theory predictions. Possible deviations are explained. The fluid is air in normal conditions. For the plate made of mylar, the following values are taken: $K_{\mathrm{s}} = 0.237\,\mathrm{W\,K^{-1}\,m^{-1}}$, $\rho_{\mathrm{s}} = 900\,\mathrm{kg\,m^{-3}}$ and $c_{\mathrm{s}} = 2700\,\mathrm{J\,K^{-1}\,kg^{-1}}$. The geometry corresponds to $y_0/\delta_\kappa = 1.9$ and $l/\delta_\kappa = 0.41$. Usually $L/\lambda = 0.0088$ unless specified otherwise. In the following, two parameters are changed: the position x_{S} of the plate center, given in the non-dimensional form kx_{S}, and the acoustic Mach number Ma.

5.1. Thermal effect at low Mach number

We first focus on the effect of the Mach number, which is first kept small, that is $Ma < 2\%$. In Fig. 9 we plot the temperature difference ΔT as a function of the

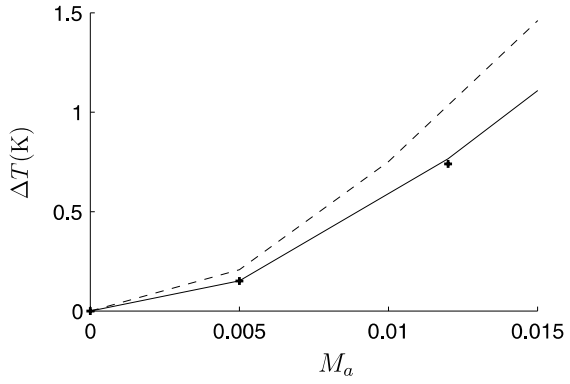

Fig. 9. Temperature difference ΔT as a function of Ma, for low values of Ma: (+) calculated, (––) linear theory (Eq. (8)) (—) modified linear theory (Eq. (25)). $kx_{\mathrm{s}} = 2.35$.

Mach number for a fixed position $kx_{\mathrm{S}} = 2.35$ of the plate, located between velocity and pressure antinodes. The temperature difference is compared to the linear theory prediction Eq. (8). We observe a deviation of about 20% even for a low value $Ma = 0.5\%$ ($D_{\mathrm{r}} = 0.7\%$) of the Mach number. If we exclude non-linear effects, two factors can explain this deviation. The first one was put forward by Kim et al. [8]: the temperature gradient is constant along the plate, except at the extremities of the plate. This is shown in Fig. 10 which provides the mean temperature along the plate obtained in the present simulation for $Ma = 0.5\%$. In this figure we see that the temperature difference ΔT that is obtained is actually less than the one ΔT_{lin} that would be obtained if the temperature gradient were constant over the whole plate length. This is not taken into account by Eq. (8). The second factor is the difference that exists between the mean temperature gradient in the fluid, and the one in the plate. In the linear theory these gradients are assumed to be equal. This assumption is not verified in the present simulation. The mean temperature T_{m} in the fluid at five different sections ($x = cst$) above the

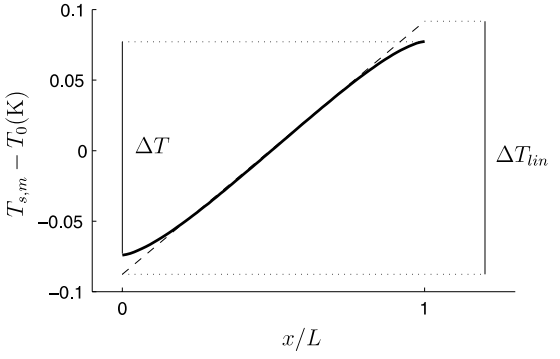

Fig. 10. Mean temperature $T_{\mathrm{sm}} - T_0$ in the solid plate. ΔT is the temperature difference between the extremities of the plate, ΔT_{lin} is the temperature difference that would exist if the mean temperature gradient were constant. $Ma = 0.5\%$, $kx_{\mathrm{s}} = 2.35$.

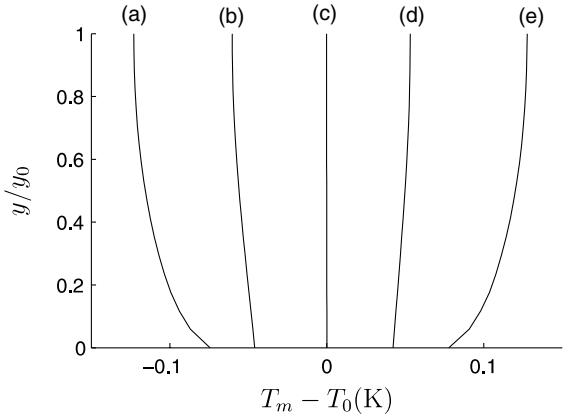

Fig. 11. Mean temperature in the fluid at five different sections of the channel above the plate: (a) section $x = x_C$ (cold side), (b) section $x = x_C + L/4$, (c) section $x = x_S$ (midsection), (d) section $x = x_C + 3L/4$, (e) section $x = x_H$ (hot section). At $y = 0$, the mean temperature corresponds to that of the plate.

plate is plotted versus the position y/y_0 in the corresponding section in Fig. 11. At $y = 0$, the mean temperature equals that of the plate. We see that the temperature is nearly uniform across the section in the central part of the plate (curves (b), (c) and (d) in Fig. 11), but not at the plate ends (curves (a) and (e)). This lack of uniformity is actually not surprising and is due to increased heat transfer between the plate and the fluid at the extremities of the plate.

To take account of the previous two observations, the expression for the conduction term $\dot{Q}_{\mathrm{m,cond}}$ appearing in the Eq. (6) must be modified according to

$$\dot{Q}_{\mathrm{cond,m}} = -Ky_0\frac{\alpha_2}{\alpha_1}\frac{\mathrm{d}T_\mathrm{m}}{\mathrm{d}x} - K_\mathrm{s}l\frac{1}{\alpha_1}\frac{\mathrm{d}T_\mathrm{m}}{\mathrm{d}x} = \frac{1}{\alpha_1}\left(-Ky_0\alpha_2\frac{\mathrm{d}T_\mathrm{m}}{\mathrm{d}x} - K_\mathrm{s}l\frac{\mathrm{d}T_\mathrm{m}}{\mathrm{d}x}\right). \quad (21)$$

The coefficient α_1 results from the variation of the mean temperature gradient within the plate at its extremities. It is given by

$$\alpha_1 = \frac{\Delta T}{\Delta T_\mathrm{lin}}. \quad (22)$$

The coefficient α_2 results from the non-uniformity of the mean temperature in the y direction. It is given by

$$\alpha_2 = \frac{\Delta T_\mathrm{av,fluid}}{\Delta T}, \quad (23)$$

where $\Delta T_\mathrm{av,fluid}$ is computed according to

$$\Delta T_\mathrm{av,fluid} = \frac{1}{y_0}\int_0^{y_0} T_\mathrm{m}(x_H, y) - T_\mathrm{m}(x_C, y)\,\mathrm{d}y. \quad (24)$$

The temperature non-uniformity in y direction implies that the mean temperature difference between the section $x = x_C$ and the section $x = x_H$, in the plate ΔT, and in the fluid $\Delta T_\mathrm{av,fluid}$, are not the same. Hence the effect of α_2 is to modify the relative importance of the return conductive fluxes within the plate and within the fluid which result from those temperature differences. This can be seen from the bottom line in Eq. (21), where α_2 would simply equal 1 if the mean temperature were uniform across the section. Injecting Eq. (21) in Eq. (6) results in a new expression for ΔT:

$$\Delta T = \alpha_1\frac{-Ly_0}{4\rho_\mathrm{m}c}P_\mathrm{A}^2\sin(2kx_\mathrm{S})A_1 \times\left[\alpha_2 y_0 K + lK_\mathrm{s} - \frac{y_0 c_p}{4\omega\rho_\mathrm{m}c^2(1-Pr)}P_\mathrm{A}^2(1-\cos(2kx_\mathrm{S}))A_2\right]^{-1}. \quad (25)$$

This expression is a slightly modified form of Eq. (8) which takes of thermal effects described just above. It must be noticed that α_1 and α_2 are not constants that are chosen in order to fit the simulation, they are rigorously computed once the simulation is performed, according to relations (22) and (23). Unfortunately they can be used only as a posteriori corrections. If an analytical a priori expression is wanted for both coefficients, an extension of the linear theory is required that would be valid at the plate ends and would give an expression for the mean temperature in the fluid and in the plate. An analysis similar to that of Mozurkewich [18] is necessary to provide an analytical expression of the form (25). But this is far from being straightforward. Data obtained using Eq. (25) are plotted in Fig. 9. We see that the modified expression Eq. (25) fits our numerical results at low Mach numbers. Hence it appears that the disagreements that may be found between simulations and the linear theory (Eq. (8)) at low Mach number are not due to non-linear effect but to thermal effects. In particular, the disagreement is not due to an error in the calculation of the thermoacoustic flux, previously noted $\dot{Q}_\mathrm{thermoac,m}$. This flux is actually well predicted by the linear theory (at least in the middle part of the plate) but an error is made in the calculation of the return conductive fluxes and more especially in the distribution of these fluxes between the plate and the fluid. This is coherent with the observations made by Piccolo et al. [10] summarized in the introduction. The error in heat fluxes distribution leads to an overprediction of ΔT in Eq. (8). Taking account of thermal effects via α_1 and α_2 leads to Eq. (25), which agrees with the results of the simulation, at least at low Mach number values. In what follows Eq. (25) is referred to as the modified linear theory.

How much the linear theory and the modified linear theory are different depends on the value of the coefficients α_1 and α_2. Fig. 12 gives the dependence of α_1 and α_2 on Ma, for two values of the plate length, $L = 0.0088\lambda$ and $L = 0.025\lambda$. In general α_1 is less than 1, and α_2 is more than 1. The more the value is close to 1, the more the linear and modified linear theories

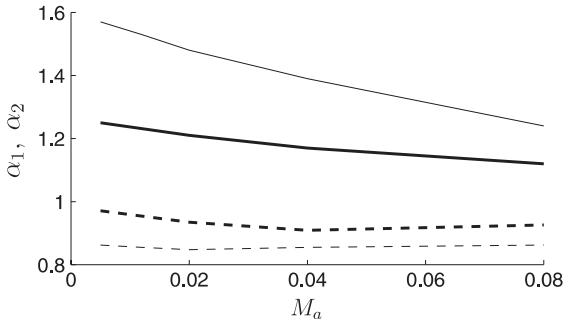

Fig. 12. Evolution of the coefficients α_1 and α_2 as a function of the Mach number, for two values of the plate length. Plate of length $L = 0.0088\lambda$: (– –) α_1, (—) α_2. Plate of length $L = 0.025\lambda$: (- -) α_1, (—) α_2. $k\ x_S = 2.35$.

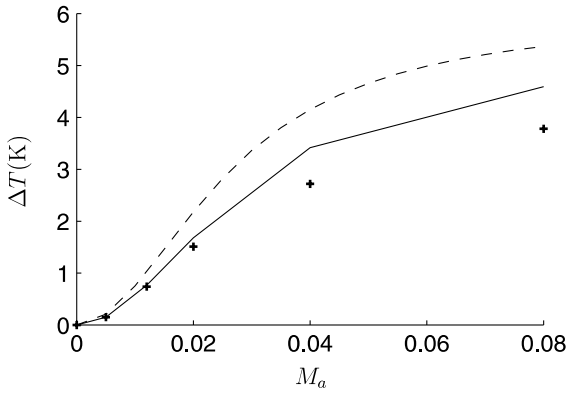

Fig. 13. Temperature difference as a function of *Ma*: (+) calculated, (– –) linear theory (Eq. (8)) (—) modified linear theory (Eq. (25)). $kx_s = 2.35$.

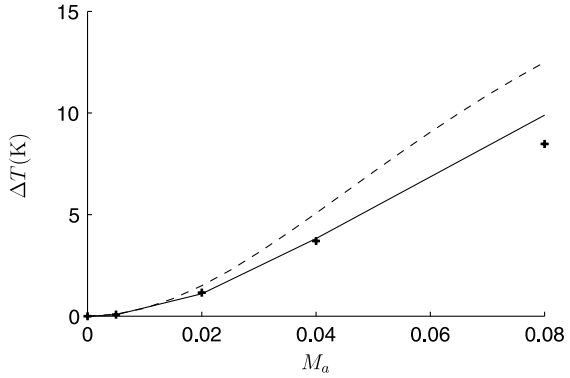

Fig. 14. Temperature difference as a function of *Ma*: (+) calculated, (– –) linear theory (Eq. (8)) (—) modified linear theory (Eq. (25)). $kx_s = 2.9$.

give similar results. We observe in Fig. 12 that α_1 is nearly constant while α_2 decreases with Mach number. When the plate length is increased the value of the coefficients approaches 1. Unfortunately, the plate length can not be increased much otherwise the short stack approximation used to derive Eq. (8) as well as Eq. (25) fails. For the shortest plate ($L = 0.008\lambda$) α_1 is about 0.9, and α_2 is about 1.4. The total error between the linear and modified linear theories is then about 20%. This value is significant but much less than the 300% value that has been reported by Kim et al. [8], Duffourd [9], and Piccolo et al. [10]. Nevertheless the values of α_1 and α_2 depend on a lot of parameters, including stack position kx_S, thermal conductivities K_s of the solid and K of the fluid, plate spacing $2y_0$, and Mach number *Ma*. This complex dependence may in some configurations lead to a high deviation between the linear theory and the modified linear theory, that is between the linear theory and simulations or measurements. There is another possible explanation for the large deviation observed by Duffourd, Kim and Piccolo. Eq. (8) or (25) are valid within the short stack approximation. The value of the plate length used by these authors ($L = 0.025\lambda$ for Duffourd and $L = 0.041\lambda$ for Piccolo) may be too long for this approximation to be valid. Hence comparisons with Eq. (8) or (25) may not be appropriate for their experiments.

In conclusion, some deviations have been observed between our simulations and the linear theory predictions (Eq. (8)). This deviation is due to thermal effects and can be taken into account using the modified linear theory (Eq. (25)). In the following, results are compared both to the linear theory and to the modified linear theory.

5.2. Non-linear effects at high Mach number

Our results are now given on the whole Mach number range, that is for Mach number up to 8%. For the same case as above, the temperature difference is plotted as a function of the Mach number for the whole Mach number range. Results are presented in Fig. 13 for $kx_s = 2.35$ and in Fig. 14 for $kx_s = 2.9$. For $kx_s = 2.35$ the simulation agrees well with the modified linear theory given by Eq. (25) for Mach number below 1.5%. Above this value a disagreement appears due to non-linear effects. More precisely, it is mostly due to the non-linear oscillation of temperature in the plate region that has been described in a previous section. In that section it was indicated that the non-linearities of temperature decrease as the plate is pushed toward the velocity antinode. A consequence of that is shown in Fig. 14: for a position $kx_s = 2.9$ closer to the velocity antinode than the previous one, the Mach number at which the temperature difference deviates from the linear theory prediction is more than 4%. This value is larger than the 1.5% value found for $kx_s = 2.35$.

At this point, it may be interesting to estimate the effect of temperature non-linearities on the performance of the device. Thus the Coefficient Of Performance

(COP) of the refrigerator was calculated numerically and was compared to the COP predicted using the linear theory. The COP is the ratio of the work flux consumed by the plate to the heat power pumped by the plate. Using the previous notations, it is

$$\mathrm{COP} = \frac{\dot{Q}_{\mathrm{thermoac,m}}}{\dot{W}_{\mathrm{m}}}. \tag{26}$$

The COP predicted by the linear theory is estimated making the boundary layer assumption, using Eq. (76) for $\dot{Q}_{\mathrm{thermoac,m}}$ and Eq. (80) for $\dot{W}_{\mathrm{m}}$, both given by Swift [1]. The ratio of the numerically calculated COP to the theoretical COP is plotted versus the acoustical Mach number in Fig. 15, in the case $kx_{\mathrm{s}} = 2.35$. At low Mach numbers, $Ma \leqslant 2\%$ (for which no non-linearity is observed, as concluded from Fig. 13) the numerically calculated COP is 95% of the theoretical COP. For higher acoustical Mach numbers, $Ma \geqslant 2\%$, the numerically calculated COP is much less than the theoretical COP. At $Ma = 8\%$, it is only about 65% of the predicted COP. From this example, it can be concluded that the apparition of temperature non-linearities can have a dramatic effect on the performance of the refrigerator. Actually, it was shown in Ref. [11], that when the temperature non-linearities appear, the heat power pumped by the plate is no more proportional to Ma^2, as expected from the non-linear theory, but to Ma.

5.3. Effect of plate position in the resonator

We now turn to the effect of the parameter kx_{s} representing the stack plate position. In Figs. 16 and 17 we plot the temperature difference ΔT as a function of kx_{s}

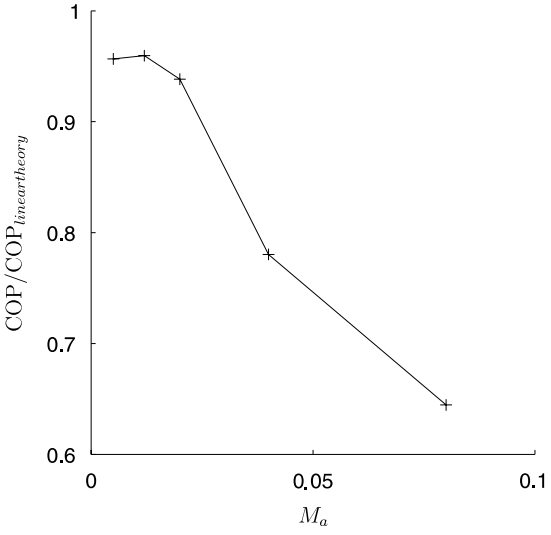

Fig. 15. Coefficient of performance normalized by the coefficient of performance predicted by the linear theory, as a function of Ma. $kx_{\mathrm{s}} = 2.35$.

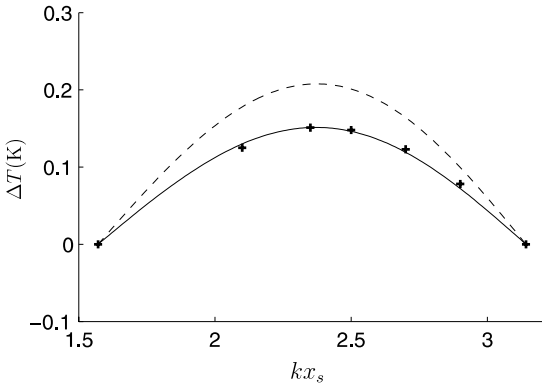

Fig. 16. Temperature difference as a function of kx_{s}: (+) calculated, (––) linear theory (Eq. (8)) (—) modified linear theory (Eq. (25)). $Ma = 0.5\%$.

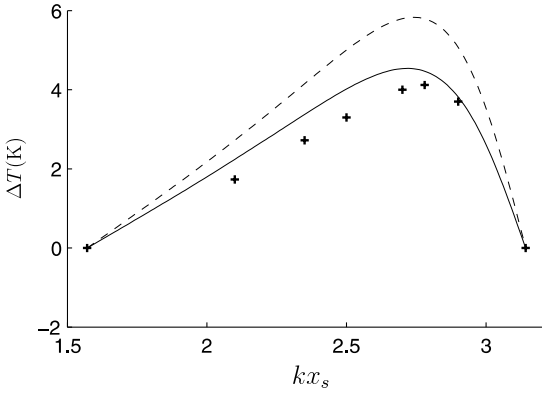

Fig. 17. Temperature difference as a function of kx_{s}: (+) calculated, (––) linear theory (Eq. (8)) (—) modified linear theory (Eq. (25)). $Ma = 4\%$.

for two values of the Mach number: $Ma = 0.5\%$, and $Ma = 4\%$. For $Ma = 0.5\%$, we observe that the temperature difference is well predicted by the modified linear theory for all plate positions (but not by the raw linear theory, Eq. (8)). In particular, the maximum temperature difference is reached for $kx_{\mathrm{s}} = 2.35$, that is, between the pressure and the velocity antinodes. For a higher value $Ma = 4\%$ of the Mach number, simulations and the modified linear theory do not agree for most values of kx_{s}, as expected at high Mach numbers for which non-linearities are obtained. The difference between the calculated curve and the modified linear theory decreases as kx_{s} increases, which was also found experimentally by Atchley et al. [6]. For a value of kx_{s} high enough, numerical results and the modified linear theory predictions even match. Again this is the case because non-linearities in temperature oscillation decrease near the velocity antinode as indicated above. From Fig. 17 a second observation can be made. The optimal value of kx_{s} for which the temperature difference is maximum is slightly larger than the one predicted by the modified

linear theory (as well as by the raw linear theory), which was also observed by Worlikar et al. [7].

6. Conclusion

The temperature difference between the extremities of a stack plate in a thermoacoustic refrigerator was calculated numerically. It was found that even at low Mach numbers, the calculated difference does not always agree with that predicted by the linear theory. Deviations up to 25% have been observed. Two reasons for these deviations have been given. First at the extremities of the plate, the mean temperature is not a linear function of the axial position. Second the mean temperature in the plate and in the fluid are not equal at the plate ends, contrary to the linear theory assumptions. Taking account of these thermal effects, a slighty modified expression for the temperature difference was proposed, which agreed well with the numerical results at low Mach numbers.

For high Mach number values, the modified linear theory predictions and numerical results do not agree. The deviation is due to non-linear effects which affect especially the temperature variation above the plate. In particular the deviation is stronger near the velocity antinode, where temperature non-linearities are themselves stronger, than near the velocity node. Some other non-linearities due to non-linear propagation in the resonator are not taken into account by the present methods and could be responsible for a even larger disagreement between the simulations and the linear theory predictions.

As was pointed out, the modified theory used in this paper could be deduced only a posteriori. A more predictive theory, taking into account the thermal effects described in this paper, may be the subject for further study.

Acknowledgment

This work were supported by DGA, computations were performed in part at IDRIS computing center.

References

[1] Swift GW. Thermoacoustic engines. J Acoust Soc Am 1988;84:1145–80.
[2] Tijani MEH, Zeegers JCH, De Waele ATAM. Design of thermoacoustic refrigerator. Cryogenics 2002;42:49–57.
[3] Tu Q, Li Q, Guo F, Wu J, Liu J. Temperature difference generated in thermo-driven thermoacoustic refrigerator. Cryogenics 2003;43:515–22.
[4] Jin T, Chen GB, Shen Y. A thermoacoustically driven pulse tube refrigerator capable of working below 120 K. Cryogenics 2001;41:595–601.
[5] Wheatley J, Hofler TJ, Swift GW, Migliori A. An intrinsically irreversible thermoacoustic heat engine. J Acoust Soc Am 1983;74:153–70.
[6] Atchley AA, Hofler TJ, Muzerall ML, Kite MD, Ao C. Acoustically generated temperature gradients in short plates. J Acoust Soc Am 1990;88:251–63.
[7] Worlikar AS, Knio O. Numerical simulation of a thermoacoustic refrigerator. Part 2: Stratified flow around the stack. J Comput Phys 1998;144:299–324.
[8] Kim YT, Suh SJ, Kim MG. Linear resonant duct thermoacoustic refrigerator having regenerator stacks. In: Proceedings of the 16th International Congress on Acoustics, June 1998, p. 821–2.
[9] Duffourd S. Réfrigérateur thermoacoustique: études analytiques et expérimentales en vue d'une miniaturisation. PhD thesis n°2001-06, Ecole Centrale de Lyon, 2001.
[10] Piccolo A, Cannistraro G. Convective heat transport along a thermoacoustic couple in the transient regime. Int J Thermal Sci 2002;41:1067–75.
[11] Marx D, Blanc-Benon Ph. Numerical simulation of the stack/heat exchanger coupling in a thermoacoustic refrigerator. AIAA J 2004;42:1338–47.
[12] Bogey C, Bailly Ch. A family of low dispersive and low dissipative explicit schemes for flow and noise computations. J Comput Phys 2004;194:194–214.
[13] Marx D. Simulation numérique d'un réfrigérateur thermoacoustique. PhD thesis, Ecole Centrale de Lyon, 2003.
[14] Chen R-L, Chen Y-C, Chen C-L, Tsai C, Denatale J. Development of miniature thermoacoustic refrigerators. AIAA Paper 2002-0206.
[15] Hamilton MF, Ilinskii YA, Zabolostkaya EA. Nonlinear two-dimensional model for thermoacoustic engines. J Acoust Soc Am 2002;111:2076–86.
[16] Atchley AA, Bass HE, Hofler TJ. Development of nonlinear waves in a thermoacoustic prime mover. In: Hamilton MF, Blackstock DT, editors. Frontiers of Nonlinear Acoustics: 12th ISNA. New York: Elsevier; 1990. p. 603–8.
[17] Gusev V, Lotton P, Bailliet H, Job S, Bruneau M. Thermal wave harmonics generation in the hydrodynamical heat transport in thermoacoustics. J Acoust Soc Am 2001;109:84–90.
[18] Mozurkewich G. Time-average distribution in a thermoacoustic stack. J Acoust Soc Am 1998;103:380–8.